Experimental particle's shapes reconstructions from their interferometric images using the Error-Reduction algorithm

Barbara Delestre, Alexis Abad, Mohamed Talbi, Michael Fromager, Marc Brunel

Version of Record: https://www.sciencedirect.com/science/article/pii/S0030401821004788
Manuscript_8a531719366ded7ea1b83efb62a01980

Experimental particle's shapes reconstructions from their interferometric images using the Error-Reduction algorithm

Barbara Delestre[1], Alexis Abad[1], Mohamed Talbi[1], Michael Fromager[2] Marc Brunel[1,*],

[1]*UMR CNRS 6614 CORIA, Université de Rouen Normandie, Avenue de l'Université, BP 12, 76801 Saint-Etienne du Rouvray Cedex, France*
[2]*UMR CNRS 6252 CIMAP, CEA, Ensicaen, Université de Caen, 6 Bd Maréchal Juin, F-14050 Caen Cedex, France*
**marc.brunel@coria.fr*

Abstract

The Error-Reduction algorithm is tested to reconstruct the exact 2D-shape of irregular rough particles from their experimental interferometric images. The particles tested are "programmable" particles generated with a digital micromirror device. The method is first applied to centrosymmetric particles, and then to non-centrosymmetric particles where the twin image problem brings additional difficulty.

I - Introduction

The detection and the characterization of irregular particles in a flow is particularly important in many domains from combustion and sprays, to meteorology, nuclear safety, cosmetics, or medicine. Contrary to classical microscopy, the goal is to observe an ensemble of submillimetric particles that cover a field of view of tens of square centimeters, while the working distance exceeds tens of centimeters. With these constraints, the ability to observe and measure precisely all particles observed with a single-shot set-up represents a challenge. Interferometric Particle Imaging (IPI) offers a solution that has been explored in the last years: from single-view to multi-views set-ups for the tomography of particles in flows [1-14]. With this technique, particles are illuminated by a nanosecond laser pulse (the velocity of the flow can thus be very important, compatible with airborne operation for example). Light is scattered by the particles in all directions. A CCD sensor associated to an imaging optics records a defocused image of each particle present in the field of view. The speckle pattern obtained for each particle is analysed for size measurement and morphological characterization. Special attention is presently paid to the reconstruction of the exact particles' shapes from their speckle patterns [8,11,12].

Let us consider an irregular rough particle of any shape under laser illumination. A priori, there is no theoretical model to predict rigorously the electromagnetic field scattered by the particle. This is particularly true in the case of ice crystals whose growth's description and shape's modelling themselves represent an intense domain of research [15,16]. Despite this lack of a rigorous light scattering description, IPI enables approximate rough particle sizing. In a simplified description indeed, the rough particle can be assimilated to an ensemble of coherent point emitters that cover the whole

particle. Using a scalar Huygens-Fresnel theory, the 2-Dimensional Fourier transform of the interferometric image of the particle is then shown to be linked to the 2D-autocorrelation of the envelope of the particle through relation (1) [5]:

$$|FT_{2D}[I](\lambda B_{tot}u, \lambda B_{tot}v)| \propto |A_{2D}[G_0](dx, dy)| \qquad (1)$$

where *I* is the intensity of the interferometric out-of-focus image of the particle and G_0 the electric field scattered by the illuminated particle (a sum of Dirac functions representing each point emitter). λ is the wavelength of the laser. λB_{tot} is the scaling factor between both functions which is deduced from the experimental set-up. This relation has been validated experimentally in different studies [5-10]. In most cases, it was done by comparison between the binarized 2D-autocorrelation of the in-focus image of a particle and the binarized 2D-Fourier transform of the interferometric image of the same particle. It has been further reproduced with "programmable" particles generated with a Digital Micromirrors Device (DMD) [17]. The "rough particles" are then made of an ensemble of on-state micromirrors, randomly located in a global envelope, i.e. the contour of the programmed particle. Consequently, this device has become a powerful tool to test image processing algorithms in different configurations, without having to "wait for particles" in the field of view of an IPI system.

In many previous studies, the use of relation (1) has been limited to the comparison of the contours of the binarized functions $|FT_{2D}[I](\lambda\, B_{tot}\, u, \lambda\, B_{tot}\, v)|$ and $|A_{2D}[G_0](dx, dy)|$. It enabled particle sizing, some particle's shape recognitions and lead to first attempts of 3D-tomography of irregular rough particles in a flow. However, the limit of these studies is that different 2D-shapes can exhibit the same 2D-autocorrelation. Recent studies showed that it should be possible to reconstruct the exact contour of the particle using the Hybrid Input-Output algorithm or a deep learning approach. In experiments, the interferometric image of a particle is recorded. It is 2D-Fourier transformed, binarized, and then assimilated to the 2D-autocorrelation of the particle's projection (according to the angle of view that is considered). If different 2D-shapes exhibit the same 2D-autocorrelation, the reconstruction is not unique. Algorithms exist that solve the phase problem and enable the reconstruction of a 2D-shape from its 2D-autocorrelation [19]. If relation (1) between both functions is not limited to the sole detection of the binarized contours of both functions involved, it can then be expected that unique reconstructions are possible from interferometric particles' images.

In this paper, we "program" different contours of rough particles using a Digital Micromirrors Device (DMD). The device is then illuminated by a coherent HeNe laser. The interferometric out-of-focus images are recorded with a CCD sensor, and 2D-Fourier transformed. A 2D-reconstruction of the particle's face is then done using the error reduction algorithm, and discussed. Section II describes the algorithm of reconstruction that has been used. Section III describes the experimental set-up, while section IV shows different examples of reconstructions from experimental interferometric images. Two cases are analysed and discussed : centrosymmetric particles and non-centrosymmetric particles where the twin-image problem appears to be an important source of noise [20,21].

II – Error reduction algorithm

The error reduction algorithm [18] is a method to solve the phase-retrieval problem. Based on the Gerchberg-Saxton algorithm [19], it permits to determine a function $f(x, y)$ from measurements that give the modulus of its 2D-Fourier transform $|F(u, v)|$.

$$F(u, v) = |F(u, v)|e^{i\psi(u,v)} = FT_{2D}[f(x, y)] \qquad (2)$$

(x, y) are the two-dimensional coordinates of the object in real space. (u, v) are the spectral coordinates after 2D-Fourier transform operation. $|F(u, v)|$ is the modulus of the Fourier transform which is known while ψ is the spectral phase that is unknown. In our case, $f(x, y)$ is the 2D-object to be found.

First a starting object $g_1(x, y)$ must be constructed. For this, an initial support S is defined. This initial support S is a binarized 2D-object. It is obtained using the tri-intersection method applied to the binarized form of the 2D Fourier transform of the interferometric speckle image [11]. This support S is then used for the construction of the starting object $g_1(x, y)$. The value of all pixels belonging to this support S (equal to 1 due to the binarisation) are replaced by the values of the corresponding pixels in the image of the 2D Fourier transform of the interferometric pattern. This last step allows faster convergence to a solution using the phase of the Fourier transform restricted to the support of the tri-intersection object. The 2D-function obtained is $g_1(x, y)$.

The error-reduction algorithm uses then a four-step process. For the k_{th} iteration, the different steps are as follows:

Step 1: $g_k(x, y)$ undergoes 2D-Fourier transform:

$$G_k(u, v) = |G_k(u, v)|e^{i\phi_k(u,v)} = FT_{2D}[g_k(x, y)] \quad (3)$$

Step 2: The experimental value of $|F(u, v)|$ (here the interferometric out-of-focus image according to the Wiener-Khintchine theorem) is substituted for $|G_k(u, v)|$, giving:

$$G'_k(u, v) = |F(u, v)|e^{i\phi_k(u,v)} \quad (4)$$

where the symbol « ' » indicates that the object is temporary, for further calculations.

Step 3: $G'_k(u, v)$ is inverse Fourier transformed:

$$g'_k(x, y) = |g'_k(x, y)|e^{i\theta'_k(x,y)} = FT_{2D}^{-1}[G'_k(u, v)] \quad (5)$$

Step 4: $g'_k(x, y)$ must then be changed so that the new estimate of the object, $g_{k+1}(x, y)$ satisfies the object constraints. $g_{k+1}(x, y)$ is therefore defined piecewise as:

$$g_{k+1}(x, y) = \begin{cases} g'_k(x, y) & \text{if } (x, y) \ni \gamma \\ 0 & \text{if } (x, y) \in \gamma \end{cases} \quad (6)$$

where γ is the domain in which $g'_k(x, y)$ does not satisfy the object constraints. A new estimate $g_{k+1}(x, y)$ is obtained and the four-step process can be repeated iteratively. The support γ is variable and recalculated at each iteration. For the first iteration, γ is equal to S, i.e. it is the same binarized object than S obtained from the tri-intersection. For the next iterations, the support γ is calculated from a threshold fixed on the estimated object $g'_k(x, y)$: if the pixels are higher than this threshold, these pixels and their first neighbors become white, otherwise they become black.

III – Experimental set-up for image acquisition

Experimentally, the interferometric images of perfectly known « programmable » particles are recorded with a CCD sensor. The system is composed of a Digital Micromirror Device (DMD) that reproduces a « rough particle » illuminated by an HeNe laser (wavelength: 632.8 nm). It is presented in figure 1. The particle is composed of the micromirrors that are programmed « on-state », i.e. that reflect the laser light into the direction of an imaging system. Other micromirrors keep « off-state » :

i.e. no reflection in the direction of the imaging system. An exemple of "programmed" particle is shown on figure 1 (top left of the figure). The imaging system records the interferometric out-of-focus image of the programmed particle. It is composed of a lens and a CCD sensor. The CCD sensors records this interferometric image, i.e. a speckle pattern as illustrated in figure 1.

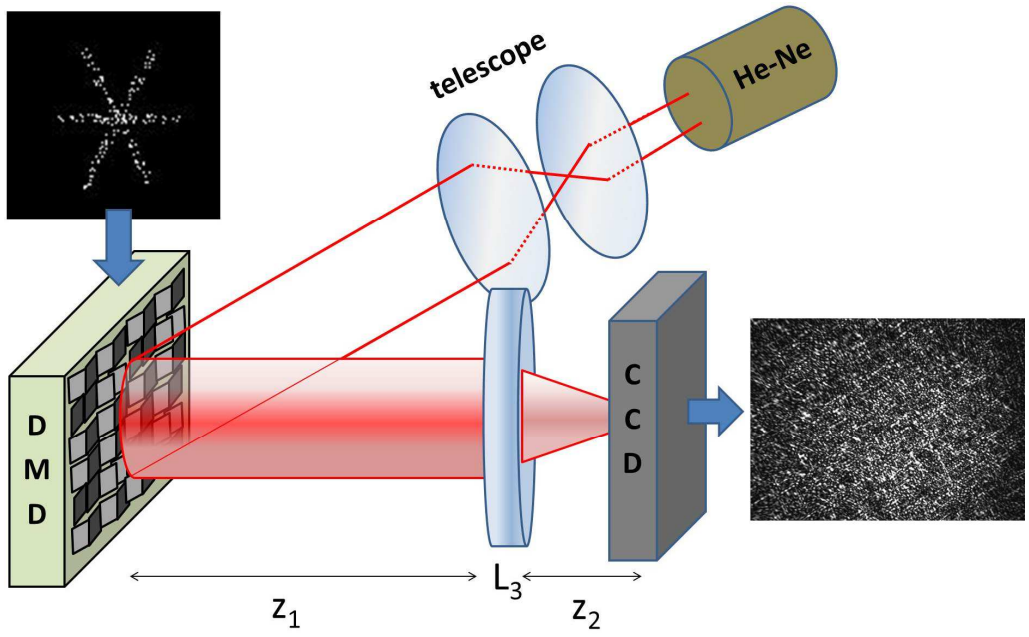

Fig. 1 : experimental set up to generate the interferometric images of « programmable » particles with a Digital Micromirror Device.

The DMD active screen used is the model DLP6500FYEHD by Texas Instruments. It has full HD resolution 1080 p (1920 × 1080 mirrors with a square geometry). The separation between the centers of two adjacent mirrors is 7.56 µm.

The imaging system is in the direction associated to the "On-State" micro-mirrors. The lens (L_3) of figure 1 is actually a Nikon objective of focus length *f = 180 mm*. Figure 1 is not at the real scale. In the set-up used, z_1=42cm, and z_2=37.5cm (using extension rings). The CCD sensor is a Thorlabs BC106N-VIS/M camera with 1360 x 1024 pixels, and a pixel size of $6.45\mu m \times 6.45\mu m$. The interferometric images that are Fourier transformed are sections composed of 680×680 pixels (of height $6.45\mu m$). The next step is the application of the scaling factor λB_{tot} for quantitative sizing. It is deduced from the experimental set-up and from the defocus parameter. The coefficient B_{tot} equals - 0.08m in this experiment.

IV- 2D-Reconstructions of the particle's face

A- Centrosymmetric particles

Let us now present some examples of reconstruction using the Error-Reduction algorithm described in section II. Figure 2(a) shows the first particle that has been programmed. It is composed of 1000 on-

state micromirrors randomly located on a cross. Figure 2(b) shows the section of its interferometric image that will be used for reconstruction. Figure 2(c) shows finally the “best” reconstructed particle. This reconstruction is obtained from the 2D-Fourier transform of the interferometric image and the application of the ER-algorithm. The scaling factor λB_{tot} has been applied on the axes of figure 2(c), according to relation (1). The axes of figures 2(a) and 2(c) can thus be directly compared. Reconstruction appears very satisfactory in this case. Figure 3(a) shows a second case where the cross has larger branches. This new programmed particle is composed of 1000 on-state micromirrors. As previously, figure 3(b) shows the section of its interferometric image obtained on the CCD sensor, and that will be used for reconstruction. Figure 3(c) shows finally the “best” reconstructed particle. We can observe that the cross is still recovered. Nevertheless, the reconstruction becomes more difficult to obtain.

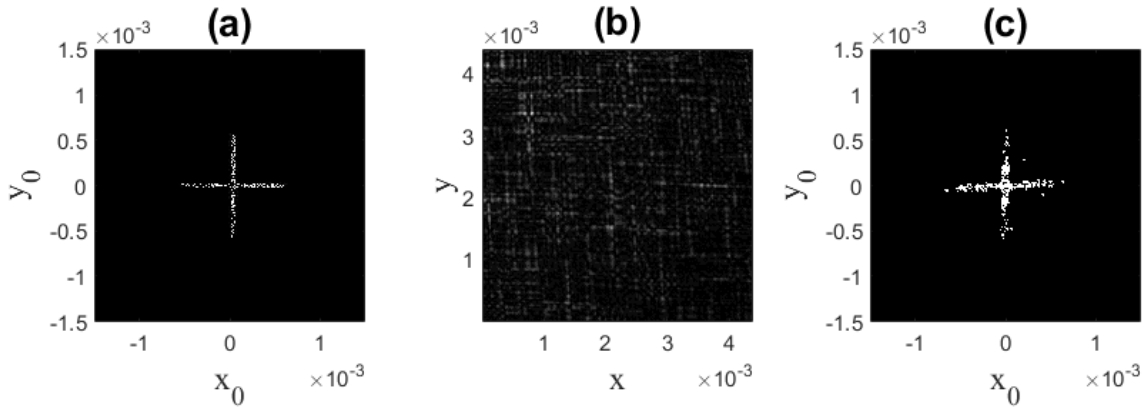

Fig. 2 : particle programmed on the DMD (a), the section of its interferometric image considered for reconstruction (b) and the reconstructed particle (c).

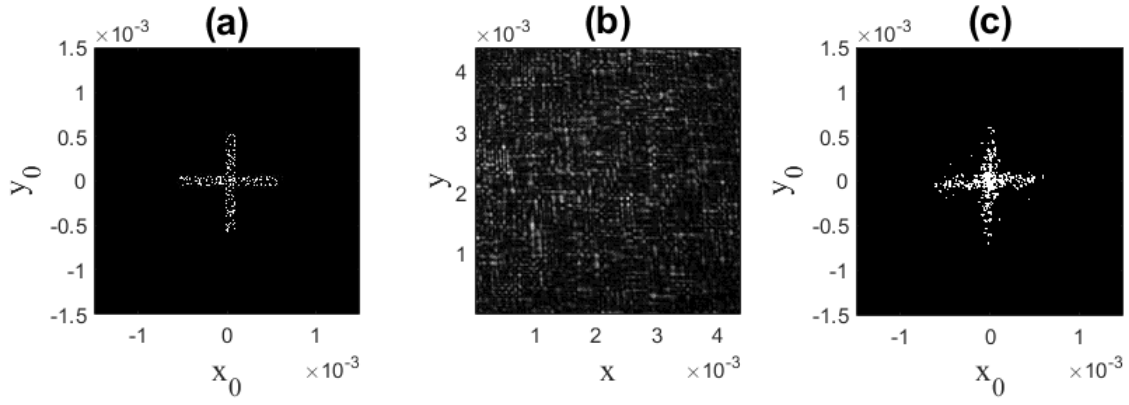

Fig. 3 : particle programmed on the DMD (a), the section of its interferometric image considered for reconstruction (b) and the reconstructed particle (c).

Let us show two other examples of reconstruction. Figure 4(a) shows a stick-like particle composed of 500 on-state micromirrors, randomly located on a stick. Figure 4(b) shows the section of its interferometric image that will be used for reconstruction. Figure 4(c) shows finally the “best” reconstructed particle. Reconstruction appears quantitatively very satisfactory again. Figure 5(a) shows a fourth case where the particle is a dendrite-like particle with six branches, composed of 2100

micromirrors. Figure 5(b) shows the section of its interferometric image, while figure 5(c) shows the best reconstructed particle. In this case again, despite some noise in the reconstructed particle, the global shape of the particle is relatively well recovered, qualitatively and quantitatively in size.

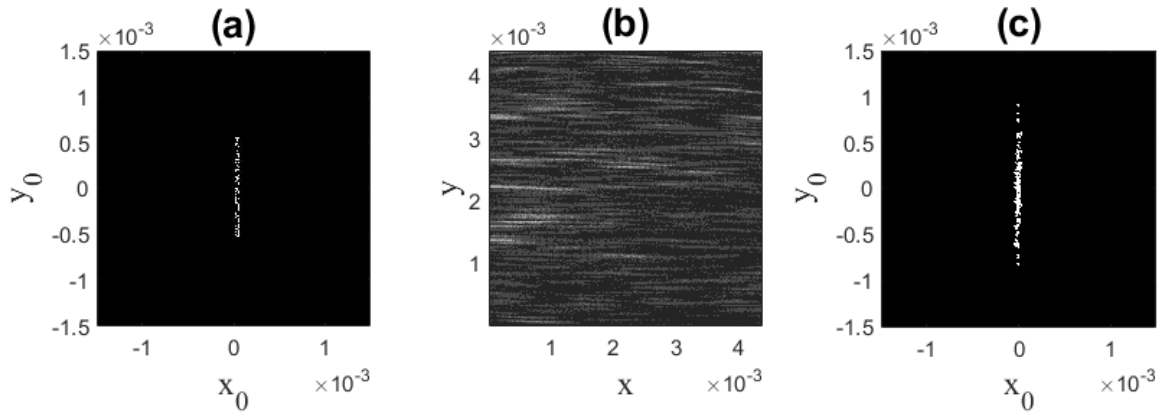

Fig. 4 : particle programmed on the DMD (a), the section of its interferometric image considered for reconstruction (b) and the reconstructed particle (c).

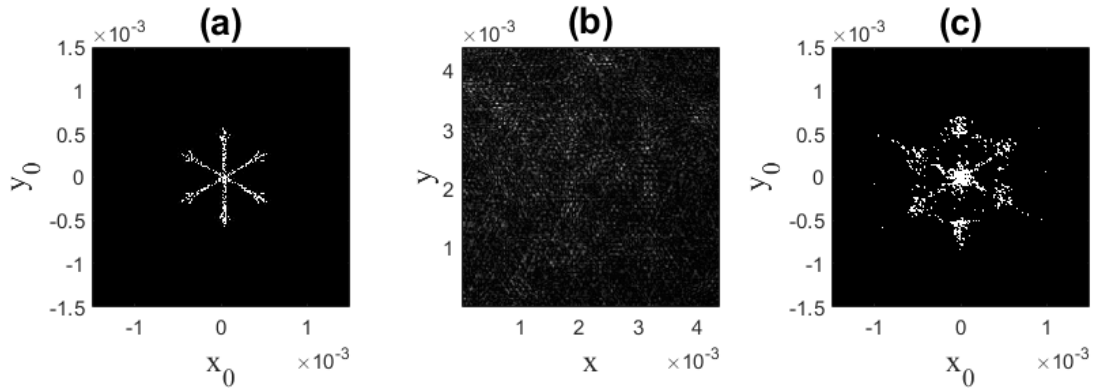

Fig. 5 : particle programmed on the DMD (a), the section of its interferometric image considered for reconstruction (b) and the reconstructed particle (c).

Figure 2(c), 3(c), 4(c) and 5(c) show that isolated pixels can be present in the reconstructed particles, and introduce noise. In the case of figure 4(c), it brings a difficulty to evaluate the exact length of the stick. This problem is clearly evidenced for the stick-like particle, but it is actually present in all cases tested: the reconstructed particles show some isolated pixels, and the addition of such pixels can enlarge more or less the contour of the reconstructed particle, depending on the threshold used in step 4 of the ER-algorithm : an object's constraint is introduced (using a threshold) to define the domain γ where $g_{k+1}(x, y)$ is set equal to zero.

The initial cause of this difficulty is that the programmed particles themselves are not plain particles, homogeneously bright. They are composed of a random repartition of micromirrors in a global envelope, which reproduces well the bright asperities of irregular rough particles under laser illumination. It appears here that the reconstruction "amplifies" this property, giving some domains

with an accumulation of bright pixels and domains where there are only a few bright pixels, which is well observed on the reconstructed dendrite on figure 5(c). Nevertheless, a useful help can be given for quantitative size measurements by the reconstruction's algorithm itself. If this threshold defined in step 4 of the ER-algorithm is very low, the algorithm leads to the reconstruction of the 2D-autocorrelation of the particle. Figure 6 illustrates the influence of this threshold: in step 4 of the algorithm (see end of section III), the definition of the new function $g_{k+1}(x,y)$ is subject to the fact that $g'_k(x,y)$ must satisfy the object's constraint. Numerically, it means that the domain γ is defined by the condition $\frac{g'_k(x,y)}{\max_{(x,y)}(g'_k(x,y))} < Th$. Figure 6(a) shows the reconstruction of the cross-like particle of figure 2 obtained when $Th = 0.45\%$. It corresponds to the best-reconstruction. Figures 6(b), (c) and (d) show then the reconstructions of the same particle obtained when $Th = 0.35\%$, $Th = 0.2\%$ and $Th = 0.08\%$. respectively. We can observe important differences between figures (a), (b) and (c). But the binarized shapes observed in figures (c) and (d) contain a very similar information although parameter Th continues to be reduced. Both figures report the 2D-autocorrelation of the initial shape of the particle.

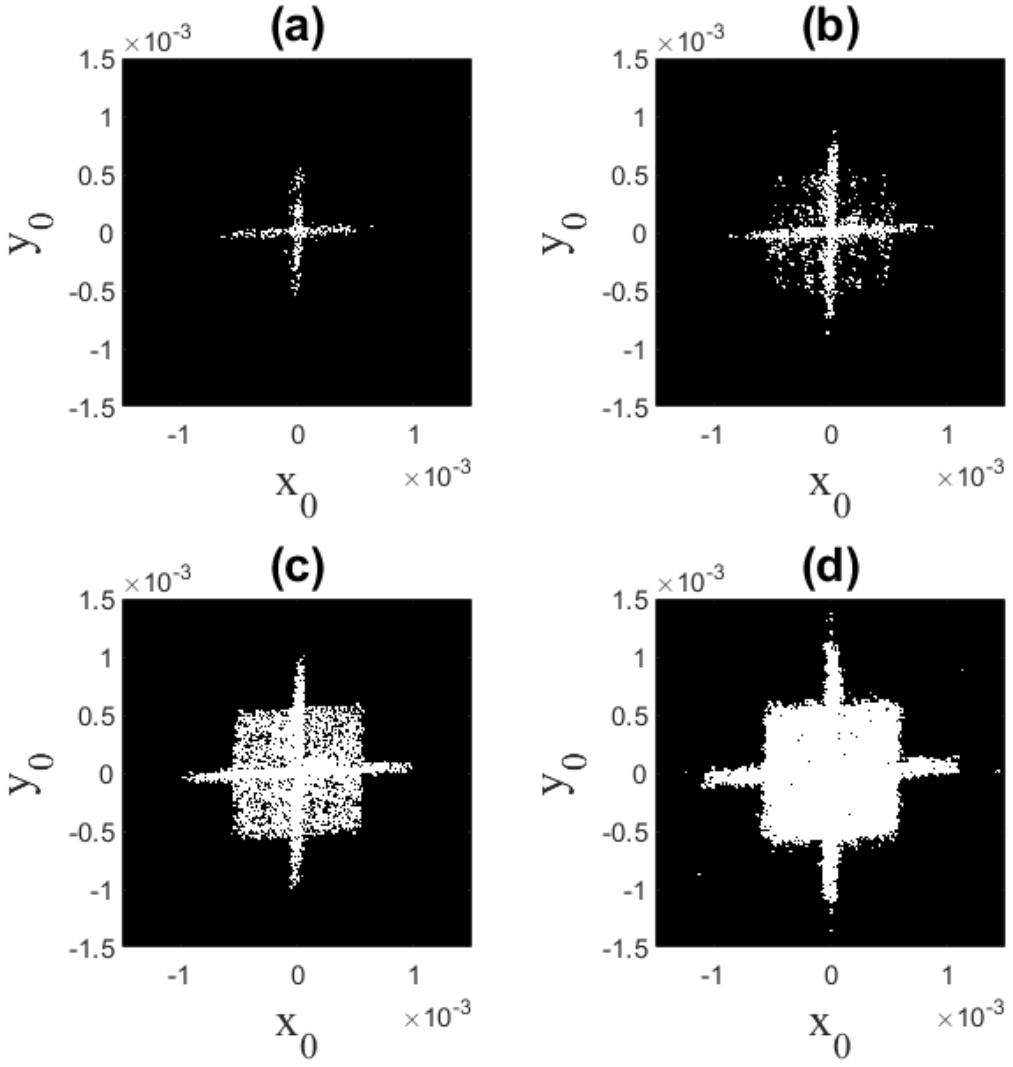

Fig. 6 : Reconstructions of the cross-like particle of figure 2, for differentvalues of the threshold Th:

$Th = 0.45\%$ in (a), 0.35% in (b), 0.2% in (c) and 0.08% in (d).

Figure 7 summarizes the low-threshold reconstructions that are obtained with the four previous particles: cross-like particles of different thicknesses in figures (a) and (b), stick-like particle in figure (c) and dendrite-like particle in figure (d). The value of the low-threshold is not a sensitive parameter of the algorithm. In the four cases presented in figure 7, the value of Th is the same : 0.15%. And the results would be very similar using $Th = 0.1\%$ or 0.2%. It is thus very easy to obtain the 2D-autocorrelation of the particles' contours precisely. But the threshold that leads to the best-reconstruction requires to be adjusted for each particle, and depends on the particle (number of micromirrors used in particular).

Let us now discuss quantitatively the best reconstructions obtained (and presented in figures 2, 3, 4 and 5). Let us consider the programmed cross-like particle shown in figure 2(a): the lengths of both horizontal and vertical branches are 1.12mm. The analysis of figure 6(a) gives an horizontal length of 1.06mm, and a vertical branch of 1.055mm (keep in mind that the 2D-autocorrelation of a rectangle is twice larger than the initial rectangle in both directions). The difference between the programmed particle and the size estimation is less than 10%. As second example, let us consider the programmed cross-like particle shown in figure 3(a): the lengths of both horizontal and vertical branches are 1.12mm again. The anlysis of figure 6(b) gives an horizontal branch of 1.07mm, and a vertical branch of 1.07mm. The difference is still very low. These low-threshold reconstructions of figure 6 are actually very powerful tools to adjust the exact constraint's threshold of the reconstruction, i.e. the one that gives the final particle's reconstructions of figures 2(c), 3(c), 4(c) and 5(c) respectively. In particular, they are very useful to identify the real sizes of particle's branches.

In summary, the ER-algorithm gives relatively good reconstructions of the initial object, although a precise size estimation can be more difficult in absence of this complementary low-threshold reconstruction. A very important criterium is the calculus time. Each reconstruction presented in this section requires only three iterations. Using a matlab code on a standard portable computer, the reconstruction from an interferometric image of 680x680 pixels requires between 30 seconds and 2 minutes (depending on the computer). This time includes the 2D-Fourier transform of the interferometric image, the initial tri-intersection to define the initial support and the iterations of the ER-algorithm.

All examples presented in this section have a common property: there are centrosymmetric. Note that such a case is not necessarily an exception in practice, depending on the family of particles that are under observation, for example ice crystals. Next section will present the case of non-centrosymmetric particles.

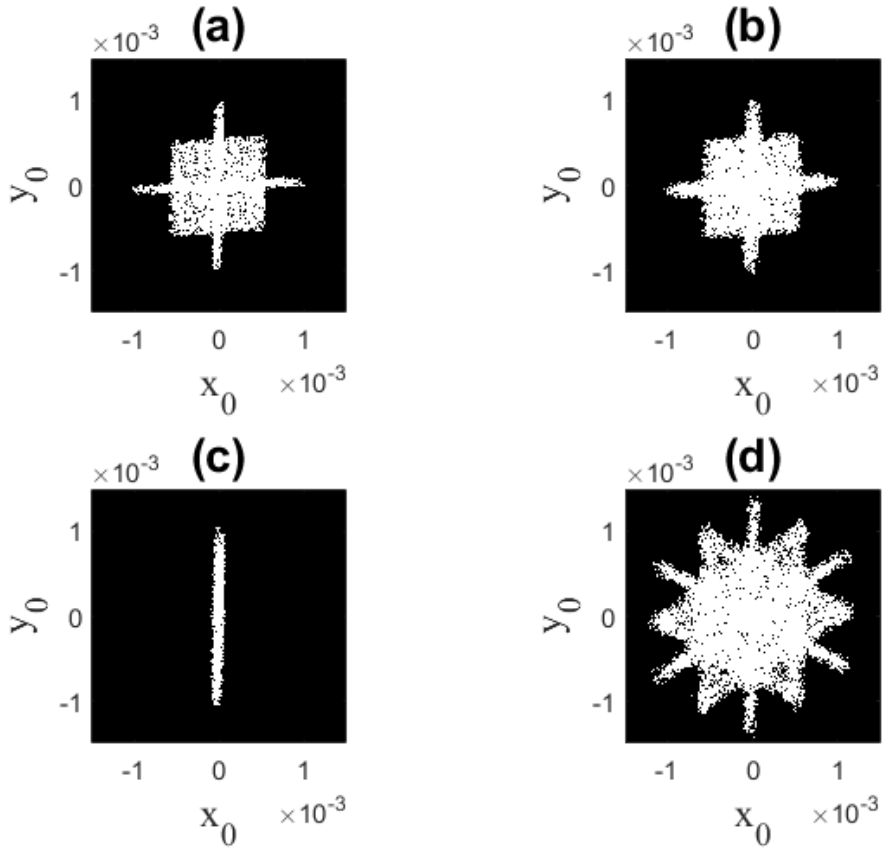

Fig. 7 : reconstructions when the constraint's threshold of the reconstruction is very low: the 2D-autocorrelation of the initial particles is then obtained: figures (a), (b), (c) and (d) must be compared to previous figures 2(c), 3(c), 4(c) and 5(c) respectively.

B- Non-centrosymmetric particles

Figure 8(a) shows a reverse Y-like particle (composed of three branches that make an angle of 120° two by two). It is composed of 1500 on-state micromirrors randomly located on the reverse Y. Figure 8(b) shows its experimental interferometric image. Figure 9(a) shows a first binarized form of the 2D-Fourier transform of the speckle pattern of figure 8(b). After tri-intersection, the initial object considered in the reconstruction process is presented in figure 9(b). Finally the "best" reconstructed particle obtained after three iterations is shown in figure 10(a). The result would be very similar after ten iterations. Reconstruction appears very different from the initial object. This is due to the non centro-symmetric shape of the particle, and the so-called "twin image" problem when using the reconstruction algorithm in this case. The algorithm does not choose between the initial Y and its centrosymmetric image. We obtain then a particle composed of 6 branches and not three. In addition the lenghs of the branches are smaller than the real ones. It is important to find tools that enable to identify this situation and correct the reconstruction, if possible. One of these tools has been presented in figure 9(b). Figure 9(b) shows indeed the initial support used in the algorithm, obtained from an initial tri-intersection. This plot gives an interesting information to identify that the particle is probably not a six-branches particle but a three-branches particle. Figure 10(b) shows the second tool. It is the low threshold reconstruction. Once again, as mentioned in figure 7 of previous section, it reproduces the 2D-autocorrelation of the initial reverse Y-like particle: it is composed of six branches whose

directions are not the ones of the three branches of the initial particle (which is perfectly normal concerning the 2D-autocorrelation of such an reverse Y-like particle). Combining the reconstruction of figure 10(a), and the informations given by figure 9(b) and 10(b), it is possible to identify a particle with three thin branches and from the length of the red arrow in figure 9(b) to have a better quantitative evaluation of the length of the branches.

It seems thus possible to “refine” the reconstruction, in order to reduce significantly the presence of the twin image. The definition of the intial support is actually very important. In a new reconstruction, we perform a more precise estimation of the binarized 2D-Fourier transform of the speckle pattern: it consists actually in a better definition of the sharp extremities of the binarized function (need evidenced by the low-threshold reconstruction of figure 10(b)). The new binarized function that will be used now is presented in figure 11(a). The better definition of the sharp extremities enables to obtain a refined support after tri-intersection: the initial support obtained, that will then be used in the reconstruction algorithm, is indeed the one of figure 11(b). After reconstruction, the best-reconstructed particle obtained after three iterations is shown in figure 11(c): the twin image is quite completely eliminated. Note that the definition of the initial support used with the ER-algorithm is the sole difference between the reconstructions of figures 10(a) and 11(c).

It is important to identify the cases where the twin image problem appears. To illustrate the identification of a case with possible confusion between two twin images, figure 12(a) reproduces the reconstructed particle (similar to figure 10(a)) while figure 12(b) gives its two-dimensional autocorrelation. Figure 12(b) shows main branches in the directions of the directions of the six reconstructed branches of the figure 12(a). This shape of figure 12(b) does not match the 2D-autocorrelation of the exact initial object : the shape should look like the one of figure 10(b) (with six branches whose directions are <u>not</u> the ones of the three branches of the initial particle).

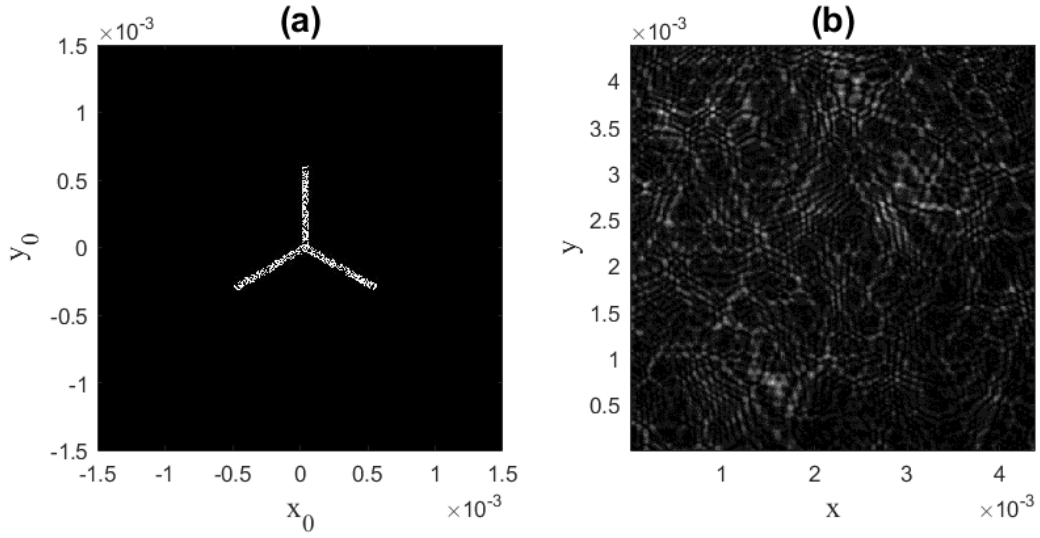

Fig. 8 : particle programmed on the DMD (a), the section of its interferometric image considered for reconstruction (b) and the reconstructed particle.

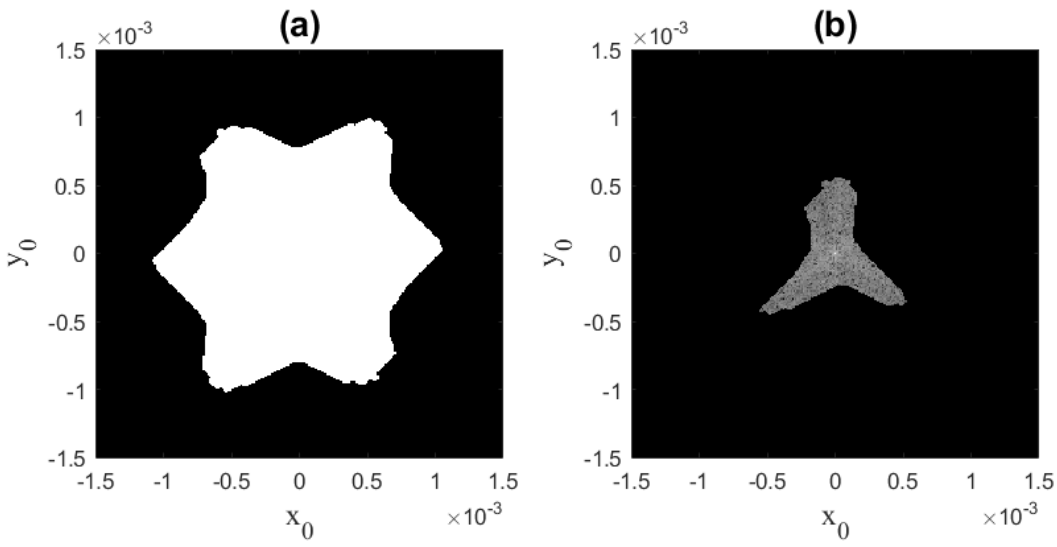

Fig. 9 : binarized 2D-Fourier transform of the interferometric image of Fig. 7(b) (a); initial support used for reconstruction (obtained after tri-intersection) (b).

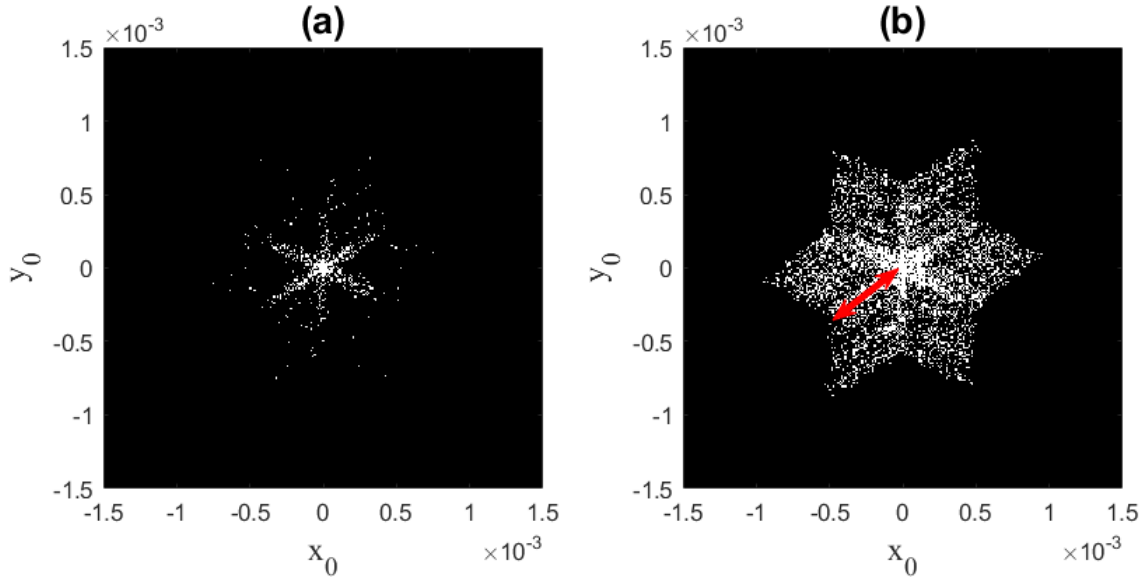

Fig. 10 : best-reconstructed particle (a); and reconstruction using a very low threshold in the ER algorithm: the 2D autocorrelation of the particle is obtained (b)

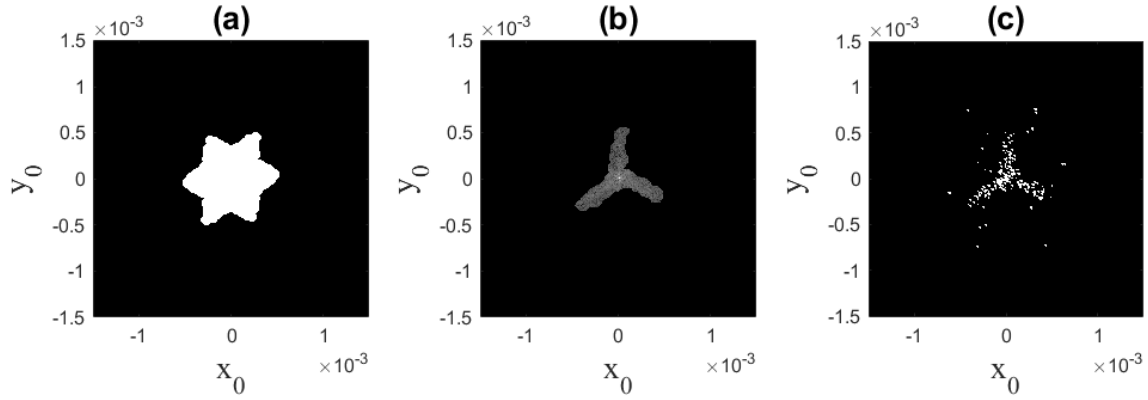

Fig. 11 : binarized 2D-Fourier transform of the interferometric image of Fig. 7(b) with better definition of the sharp extremities (a); initial support used for reconstruction (obtained after tri-intersection) (b), and best-reconstructed particle (c);

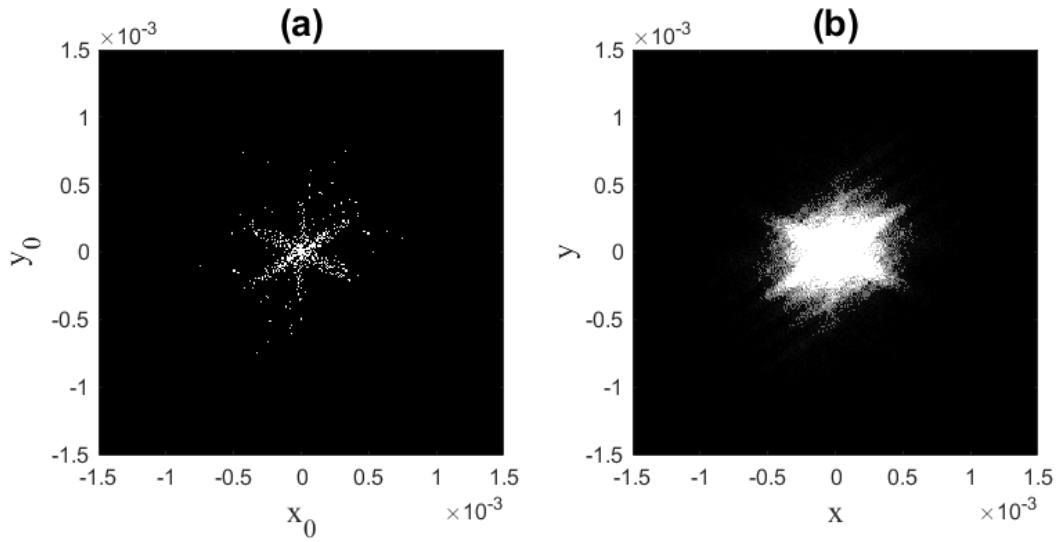

Fig. 12 : best-reconstructed particle in presence of its twin image (a); and 2D autocorrelation of the false particle obtained (b)

To confirm the efficiency of the algorithm with non-centrosymmetric particles, we have tested other shapes of particles as a L-like and a T-like particle. The results are presented in figures 13, 14 and 15. They all show the particle programmed on the DMD (subfigure (a)), and the best-reconstructed particle using the ER-algorithm (subfigure (b)). The results appear quantitatively very satisfactory. The twin-image could be eliminated in the three cases. The sticks forming the branches of the particles can be slightly thicker than the sticks of the initial programmed objects, but the lengths of the different branches are well respected. The difference between the programmed particle and the size estimation can reach here 15% (vertical branch of the T-like particle). In the case of this T-like particle (figure 15(b)), a small part of the twin image is still present on the top of the vertical branch indicating that it could not be perfectly eliminated.

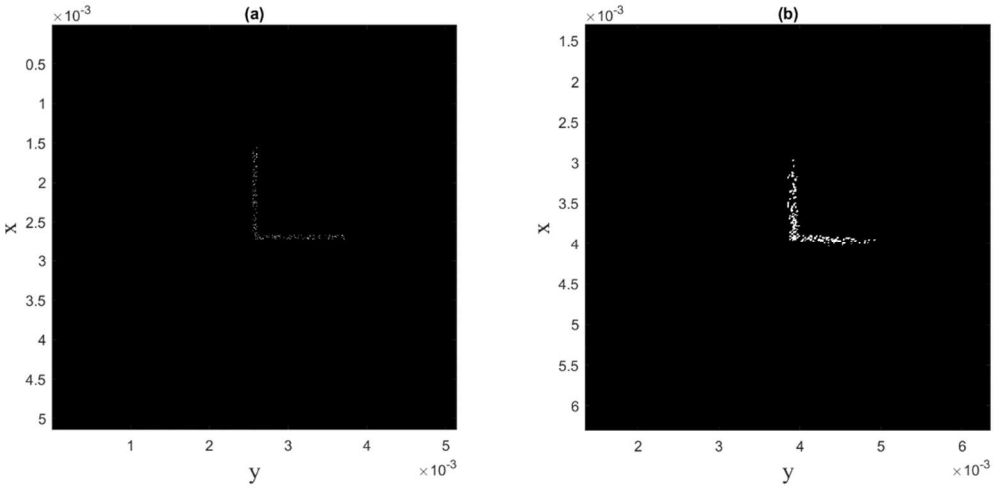

Fig. 13 : L-like particle programmed on the DMD (a), and best-reconstructed particle (b);

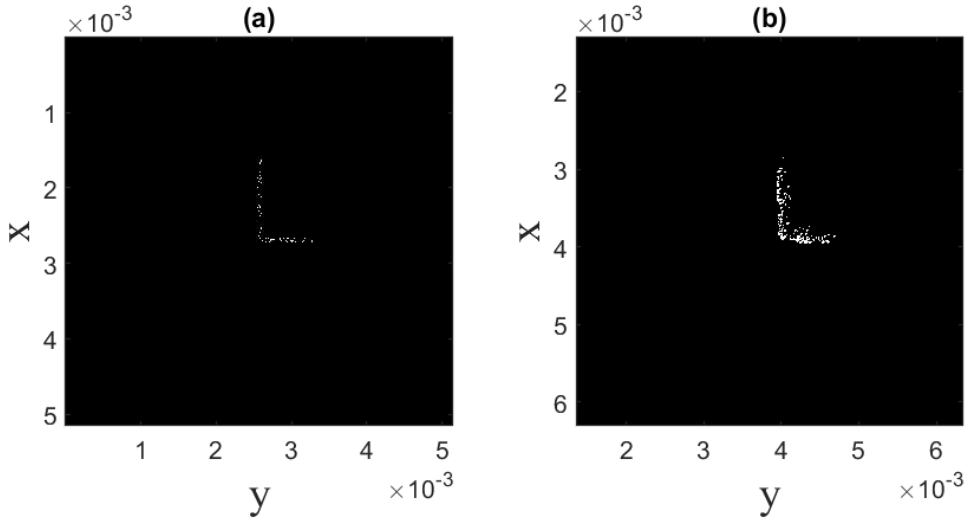

Fig. 14 : L-like particle programmed on the DMD (a), and best-reconstructed particle (b);

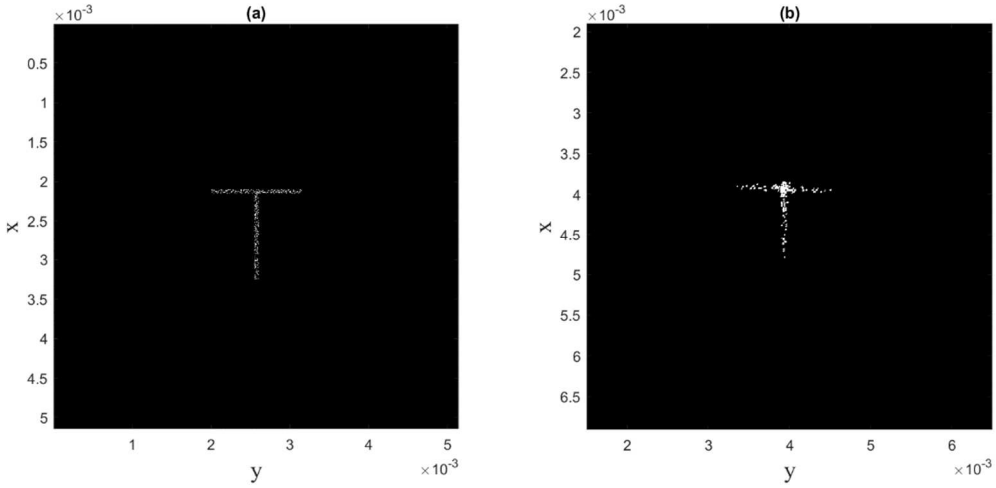

Fig. 15 : T-like particle programmed on the DMD (a), and best-reconstructed particle (b);

V – Conclusion

The Error-Reduction algorithm can thus be used to reconstruct the exact 2D-shape of irregular rough particles from their experimental interferometric images. All interferograms tested in this paper are original experimental data. The particles are “programmable” particles generated with a digital micromirror device. In the case of non-centrosymmetric particles, the twin image problem brings an important difficulty that can be addressed with a very careful definition of the initial support. This kind of reconstructions should be very powerful to realize the 3D-tomography of rough particles in a flow without shape’s ambiguity [13].

References

[1] G. König, K. Anders, A. Frohn, A new light-scattering technique to measure the diameter of periodically generated moving droplets, J. Aerosol Sci. 17 (1986) 157–167.
[2] R. Ragucci, A. Cavaliere, P. Massoli, Drop sizing by laser light scattering exploiting intensity angular oscillation in the Mie regime, Part. Part. Syst. Charact. 7 (1990) 221–225.
[3] A. R. Glover, S. M. Skippon, R. D. Boyle, Interferometric laser imaging for droplet sizing: a method for droplet-size measurement in sparse spray systems, Appl. Opt. 34 (1995) 8409–8421.
[4] H.E. Albrecht, M. Borys, N. Damaschke, C. Tropea, Laser Doppler and Phase Doppler Measurement Techniques, Springer Verlag, Berlin, 2003.
[5] M. Brunel, S. González Ruiz, J. Jacquot, J. van Beeck, On the morphology of irregular rough particles from the analysis of speckle like interferometric out-of-focus images, Opt. Commun. 338 (2015) 193–198.
[6] J. Jacquot-Kielar, P. Lemaitre, C. Gobin, Y. Wu, E. Porcheron, S. Coetmellec, G. Gréhan, M. Brunel, Simultaneous interferometric in-focus and out-of-focus imaging of ice crystals, Opt. Commun. 372 (2016) 185–195.
[7] S. G. Ruiz, J. van Beeck, Sizing of sand and ash particles using their speckle pattern: influence of particle opacity, Exp. Fluids 58 (2017) 100–108.
[8] L. Ouldarbi, M. Talbi, S. Coëtmellec, D. Lebrun, G. Gréhan, G. Perret, M. Brunel, 3D-shape recognition and size measurement of irregular rough particles using multi-views interferometric out-of-focus imaging, Appl. Opt. 55 (2016) 9154–9159.
[9] X. Wu, L. Shi, Z. Lin, Y. Wu, M. Brunel, J. Jacquot, G. Gréhan, Dual-beam interferometric particle imaging for size and shape characterization of irregular coal micro-particle: validation with digital inline holography, J. Quantum Spectrosc. Radiat. Transfer 241 (2020) 106728.
[10] Y. Wu, Y. Gong, L. Shi, Z. Lin, X. Wu, C. Gong, Z. Zhou, Y. Zhang, Backward interferometric speckle imaging for evaluating size and morphology of irregular coal particles, Opt. Commun. 491 (2021) 126957.
[11] H. Shen, L. Wu, Y. Li, W. Wang, Two-dimensional shape retrieval from the interferometric out-of-focus image of a nonspherical particle – Part I:theory, Appl. Opt. 57 (2018) 4968-4976.
[12] H. Zhang, Z. Li, J. Sun, Y. Fu, D. Jia, T. Liu, Characterization of particle size and shape by an IPI system through deep learning, J. Quantum Spectrosc. Radiat. Transfer 268 (2021) 107642.
[13] M. Brunel, B. Delestre, M. Talbi, M. Fromager, Interferometric imaging for the tomography of rough particles in a flow: A case study, Opt. Commun. 479 (2021) 126412.
[14] E. Porcheron, P. Lemaitre, J. van Beeck, R. Vetrano, M. Brunel, G. Gréhan, L. Guiraud, Development of a spectrometer for the airborne measurement of droplet sizes in clouds, J. Eur. Opt. Soc. 10 (2015) 15030.
[15] K.G. Libbrecht, The physics of snow crystals. Rep. Prog. Phys. 68 (2005) 855.
[16] G. Demange, H. Zapolsky, R. Patte, M. Brunel, A phase field model for snow crystal growth in three dimensions. NPJ: Comput. Mat. 3 (2017) 15.
[17] M. Fromager, K. Aït Ameur, M. Brunel, Digital micromirror device as programmable rough particle in interferometric particle imaging, Appl. Opt. 56 (2017) 3594-3598.
[18] R. Fienup, T.R. Crimmins, W. Holsztynski, Reconstruction of the support of an object fro the support of its autocorrelation, J. Opt. Soc. Am. 7 (1982) 3-13.
[19] R. W. Gerchberg, W. O. Saxton, A practical algorithm for the determination of phase from image and diffraction plane pictures, Optik 35 (1972) 237-246.

[20] M. Guizar-Sicairos, J. Fienup, Understanding the twin-image problem in phase retrieval, J. Opt. Soc. Am. A 29 (2012) 2367-2375.
[21] S. Kumar Gautam, R. Kumar Singh, C.S. Narayanamurthy, D. N. Naik, Single-shot and twin-image free unique phase retrieval using an aspect of autocorrelation that considers the object asymmetry, J. Opt. Soc. Am. A 37 (2020) 1826-1831.